ORIGINAL PAPER

Explicit mixed strain-displacement finite element for dynamic geometrically non-linear solid mechanics

**N. M. Lafontaine · R. Rossi · M. Cervera ·
M. Chiumenti**

Abstract Low-order finite elements face inherent limitations related to their poor convergence properties. Such difficulties typically manifest as mesh-dependent or excessively stiff behaviour when dealing with complex problems. A recent proposal to address such limitations is the adoption of mixed displacement-strain technologies which were shown to satisfactorily address both problems. Unfortunately, although appealing, the use of such element technology puts a large burden on the linear algebra, as the solution of larger linear systems is needed. In this paper, the use of an explicit time integration scheme for the solution of the mixed strain-displacement problem is explored as an alternative. An algorithm is devised to allow the effective time integration of the mixed problem. The developed method retains second order accuracy in time and is competitive in terms of computational cost with the standard irreducible formulation.

Keywords Explicit · Mixed formulation ·
Displacement-strain formulation

Nomenclature

$(\bullet) : (\bullet)$	Double contraction of tensor (inner product).
$(\bullet) \cdot (\bullet)$	Single contraction of vector and tensor.
$(\bullet)^T$	Vector, matrix transpose.

N. M. Lafontaine (✉) · R. Rossi · M. Cervera · M. Chiumenti
Universidad Politècnica de Catalunya (UPC),
Campus Norte UPC, 08034 Barcelona, Spain
e-mail: maireni@cimne.upc.edu
URL: http://www.cimne.upc.edu

N. M. Lafontaine · R. Rossi · M. Cervera · M. Chiumenti
Centre Internacional de Mètodes Numèrics en Enginyeria (CIMNE),
Universidad Politècnica de Catalunya (UPC), Campus Norte UPC,
08034 Barcelona, Spain

$(\bullet)_n$	Variable $(\bullet)$ at time t_n.
$\boldsymbol{\gamma}$	Vector of strain weighting function.
$\boldsymbol{\sigma}$	Stress tensor.
$\boldsymbol{\varepsilon}$	Small strain tensor.
$\boldsymbol{E}$	Green-Lagrange strain tensor.
$\boldsymbol{e}$	Almansi strain tensor.
$\boldsymbol{F}$	Gradient deformation tensor.
$\boldsymbol{N}$	Vector of displacement shape functions.
$\boldsymbol{u}$	Displacement field.
$\boldsymbol{w}$	Vector of displacement weighting functions.
$(\ddot{\bullet})$	Second derivative of $(\bullet)$ with respect to time t.
Δt	Time step.
δ_{ij}	Kronecker's symbol.
$\mathcal{P}$	Projection operator.
$\mathcal{P}^\perp$	Orthogonal projection operator.
$\nabla(\bullet)$	Gradient operator.
$\nabla \cdot (\bullet)$	Divergence operator.
$\nabla^s(\bullet)$	Symmetric gradient operator $\nabla^s(\bullet) = \frac{1}{2}(\nabla(\bullet) + \nabla(\bullet)^T)$.
ρ	Density.
τ_ε	Stabilization parameter.
υ	Poisson's ratio.
$\widetilde{\varepsilon}$	Enhancement strain.
E	Young's modulus.
h^e	Finite element characteristic length.
l^e_{min}	Minimum element length in the finite element mesh.

1 Introduction

The solution of problems in solid mechanics has been one of the main driving forces of the development of the finite element method (FEM), which in turn has allowed engineers to tackle a wide variety of otherwise untreatable problems. In

structural mechanics, displacements are normally chosen as unknowns and strains are computed as dependent variables by differentiation of the displacement field. Since no further reduction is possible in the choice of the unknown field, standard displacement-based approaches are also known as *irreducible formulations*. Irreducible formulations are very effective in addressing a wide range of practical problems, however, they may lead to stiff or mesh-dependent behaviour in corner cases. The performance of standard low-order displacement-based elements is also known to be poor in nearly incompressible conditions. Standard low-order elements tend to show "volumetric locking" which manifests as unrealistically stiff behaviour. A vast literature exists proposing cures for such problems, with early proposals based on reduced integration techniques or on the use of corrected assumed-strains, see for instance, the F-bar method [1]. Mixed displacement-pressure approaches started to be employed in the 90 s for the solution of truly incompressible problems [1–5]. Such techniques were also shown to provide an accuracy advantage when used in application to compressible problems (see e.g. [6]).

A different *mixed formulation* is employed here with the goal of improving the accuracy of the Finite Element discretization. The idea is to combine different primary variables, in our case displacements and strains, following the concept described in [7]. This approach was proved to show better mesh independence properties while providing the formal guarantee of a strain field converging at the same rate as the displacement one, which manifests in enhanced stress/analysis accuracy in both linear and non-linear analyses [8]. Following the ideas in [9–14], a stabilization technique is needed to allow the use of the same order of interpolation for the two primary variables of interest. Specifically the variational multiscale method (VMS) is employed in the current work.

The inherent limitation of the displacement-strain technology is related to its computational cost, since such technique involves higher number of degrees of freedom (*dofs*) per mesh node (9 vs. 3 for the 3D case) which results in much larger linear systems to be solved. The goal of the current paper is to obviate this limitation by exploring the use of an explicit time integration scheme. We will prove that a completely explicit approach is feasible when employing the mixed technology of interest and that it is competitive with the irreducible case. In particular, we will show that, for a given mesh, the critical time step is larger for the mixed formulation with respect to the irreducible case, thus enlarging the stability region of the explicit scheme. For this purpose, three different cases are studied. First a simple small-displacement example is analysed with the aim of obtaining an analytical estimation of the critical time step. Second, a cantilever beam is studied, again in the small strain regime. Lastly, the same analysis is performed in the large-

deformation regime, proving that geometrical nonlinearities can be included within the proposed mixed-displacement formulation, and that such extension comes very natural when an explicit integration scheme is employed.

2 Mixed strain/displacement formulation in transient dynamics problems

2.1 Continuous problem

The standard approach in computational solid mechanics is the use of irreducible formulations, in which the deformation is expressed in terms of the derivatives of the displacement field. While this approach is sufficient to satisfactorily address many problems, it suffers from severe limitations when used in combination with low-order finite element discretization. This is evident, for example, in the case of crack-propagation problems, which require guarantee on the local convergence of the strain field, which can not be provided by the standard irreducible element technology. Similar requirements exist however in other areas of application, such as when approaching the incompressible limit.

An appealing possibility to overcome such limitations is the use of mixed formulations, in which additional fields are used as primary variables in combination with the displacement field. Among the many existing possibilities is the use of the two primary variables $u(x)$ and $\varepsilon = \varepsilon(x)$, where $u(x)$ is the displacement field and $\varepsilon(x)$ is a suitable strain measure (e.g the linear strain $\nabla^s u$ in small deformations or the Almansi strain in the large deformations case), has appealing properties. The mixed formulation is constructed by observing that, *at continuous level*, the primal variable ε (we omit whenever possible the dependence on x) coincides with the equivalent strain $\varepsilon(u)$ computed by differentiation of the displacement field. Combining this with the linear momentum conservation equation yields

$$\nabla \cdot \boldsymbol{\sigma} + \boldsymbol{b} = \rho \ddot{\boldsymbol{u}} \quad \text{in } \Omega$$
$$-\boldsymbol{\varepsilon}(\boldsymbol{x}) + \boldsymbol{\varepsilon}(\boldsymbol{u}) = \boldsymbol{0} \quad \text{in } \Omega \tag{1}$$

where Ω is the domain occupied by the solid in a space of n_{dim} dimensions, ρ denotes the material density, the superposed dots on u denotes partial differentiation respect to time t (in this case acceleration) and $\boldsymbol{\sigma}$ is the appropriate stress tensor field, which is generally written as

$$\boldsymbol{\sigma} = \boldsymbol{C}(\boldsymbol{\varepsilon}) : \boldsymbol{\varepsilon} \tag{2}$$

where $\boldsymbol{C}$ is a fourth-order constitutive tensor, which may include non-linear behaviour. In addition to Eq. (1), which must hold for all time t, the problem is subjected to appropriate Dirichlet and Neumann boundary conditions applied respectively on the portions $\partial\Omega_u$ and $\partial\Omega_\sigma$ of the boundary, and to the initial conditions expressed by

$$\dot{u}|_{t=0} = v_0 \tag{3}$$

$$u|_{t=0} = u_0 \tag{4}$$

Introducing Eq. (2) in Eq. (1), the strong form becomes

$$\nabla \cdot (C(\varepsilon) : \varepsilon) + b = \rho \ddot{u} \quad \text{in } \Omega$$
$$-\varepsilon(x) + \varepsilon(u) = 0 \quad \text{in } \Omega \tag{5}$$

The two fields $u = u(x)$ and $\varepsilon = \varepsilon(x)$ can be both discretized by the FEM as independent primary variables. Introducing the discrete nodal unknown u_h and ε_h and the corresponding test functions w_h and γ_h and applying the Galerkin procedure we thus obtain

$$\int_\Omega w_h \cdot (\nabla \cdot (C(\varepsilon_h) : \varepsilon_h)) \, d\Omega + \int_\Omega w_h \cdot b d\Omega$$
$$= \int_\Omega \rho w_h \cdot \ddot{u}_h d\Omega \tag{6a}$$

$$\int_\Omega \gamma_h \cdot (\varepsilon_h - \varepsilon(u_h)) \, d\Omega = 0 \tag{6b}$$

Unfortunately, if equal-order interpolation are used for u_h and ε_h, the resulting Galerkin method is unstable [15]. Lack of stability manifests as a spurious oscillations in the displacements field that may entirely pollute the solution. A modified formulation needs to be devised to properly stabilize the solution, hence guaranteeing the convergence of the method. Such stabilizations can be derived in the framework of sub-grid approaches [11] as we show next.

2.2 Stabilized finite element methods

The origin of the instabilities of the proposed mixed method is that the finite element space employed is not sufficiently large to accommodate the optimal solution. Sub-grid scale stabilization methods retrofit this situation by enlarging the search space, via the introduction of sub-grid variables. The key idea of the sub-grid approach is exactly to consider that the continuous fields can be split in two components, a coarse one, to be solved for, and a finer one to be modelled. Such components correspond to different scales or levels of resolution [7], and are naturally separated in the scales that can be resolved by the finite element discretizations and the ones that can not be resolved at the given discretization level. For the stability of the discrete problem, it is necessary to include the effects of both scales in the approximation, that is, the effect of the finer (unresolved) scale needs to be included in the resolved model. For the specific problem at hand we apply such scale separation to the strain variable to give

$$\varepsilon(x) = \varepsilon_h(x) + \widetilde{\varepsilon} \tag{7}$$

where ε_h is the strain component of the (coarse) finite element scale and $\widetilde{\varepsilon}$ is the enhancement of the strain field corresponding to the sub-grid scale. While a similar assumption can be made for the displacements, previous experience (see

e.g.[7,8,15]) hints that this splitting is not needed for this variable. Taking into account such considerations, the stabilized model is in the form

$$\int_\Omega w_h \cdot \left(\nabla \cdot \left(C(\varepsilon_h) : (\varepsilon_h + \widetilde{\varepsilon})\right)\right) d\Omega$$
$$+ \int_\Omega w_h \cdot b d\Omega = \int_\Omega \rho w_h \cdot \ddot{u}_h d\Omega \tag{8}$$

$$\int_\Omega \gamma_h \cdot \left(\varepsilon_h + \widetilde{\varepsilon} - \varepsilon(u_h)\right) d\Omega = 0 \tag{9}$$

substituting $C(\varepsilon_h)$ instead of $C(\varepsilon_h + \widetilde{\varepsilon})$ (see [7,8,15]). Next a model needs to be chosen for $\widetilde{\varepsilon}$. Following the idea of Orthogonal Subscale Stabilization (OSS), we assume that the subgrid strain is proportional to the orthogonal projection of the coarse scale residual, that is, the strain residual ($r_\varepsilon := \varepsilon(u_h) - \varepsilon_h$) is introduced, and

$$\widetilde{\varepsilon} = \tau_\epsilon \mathcal{P}^\perp(r_\varepsilon) \tag{10}$$

here $\mathcal{P}^\perp$ indicates the *orthogonal projection operation* (such that $\mathcal{P}^\perp(\bullet) = \mathcal{I} - \mathcal{P}(\bullet)$ and $\mathcal{P}^\perp(\varepsilon_h) = 0$) and τ_ϵ is the algorithmic stabilization parameter, theoretically defined as

$$\tau_\epsilon = c_\varepsilon \frac{h}{L} \tag{11}$$

with c_ε, h and L being an "arbitrary" algorithmic constant, the element size and the characteristic length of the computational domain respectively. For simplicity, in the case of constant meshes it is customary to take a constant value of the stabilization parameter[8,15]. In this work typical values, in the range 0.1–0.5, were considered in all the examples. Taking into account such definition, Eq. (10) gives

$$\widetilde{\varepsilon} = \tau_\epsilon(r_\varepsilon - \mathcal{P}(r_\varepsilon))$$
$$= \tau_\epsilon(\varepsilon(u_h) - \varepsilon_h - \mathcal{P}(\varepsilon(u_h)) + \mathcal{P}(\varepsilon_h))$$
$$= \tau_\epsilon(\varepsilon(u_h) - \mathcal{P}(\varepsilon(u_h))) \tag{12}$$

Replacing into Eq. (6a) and simplifying we obtain

$$\varepsilon_h = \mathcal{P}(\varepsilon(u_h)) \tag{13a}$$

$$\varepsilon^{stab} = (1 - \tau_\epsilon)\varepsilon_h + \tau_\epsilon \varepsilon(u_h) \tag{13b}$$

$$\int_\Omega \rho w_h \cdot \ddot{u}_h d\Omega + \int_\Omega \nabla^s w_h : \left(C(\varepsilon_h) : \left(\varepsilon^{stab}\right)\right) d\Omega$$
$$= \int_\Omega w_h \cdot b_h d\Omega + \int_{\partial\Omega} w_h \cdot t_h d\Gamma \tag{13c}$$

which define the *stable* discrete problem to be solved. Note that the term added in Eq. (13b) to secure a stable solution decreases rapidly upon mesh refinement, since $\|\varepsilon(u_h) - \varepsilon\| \to 0$.

2.2.1 Remark: projection operations

It is interesting to make a short remark about the practical meaning of the orthogonal projection operator. A projector $\mathcal{P}$ is a linear operator which takes a variable defined in a given space and gives the best representation of such variable in the target space. As a requirement, a projector must comply with the property $\mathcal{P}(\boldsymbol{y}) = \mathcal{P}(\mathcal{P}(\boldsymbol{y}))$ which tells that the projection of a projected value is the projected value itself. A nonorthogonal projection of $\boldsymbol{y}$ onto the FE space is nothing more than its FE discretized value, that is, $\boldsymbol{y}_h = \mathcal{P}(\boldsymbol{y})$. Clearly the "best" FE approximation of a finite element value is the value itself, hence $\boldsymbol{y}_h = \mathcal{P}(\boldsymbol{y}_h)$ is trivially verified. If we take into account the intuitive definition of projection and we take as "best" a least-square approximation, we can readily see that the projected value $\boldsymbol{y}_h$ can be obtained as

$$\int_{\Omega} \boldsymbol{w}_h \cdot (\boldsymbol{y}_h - \boldsymbol{y}(\boldsymbol{x})) \, d\Omega = \boldsymbol{0} \tag{14}$$

which gives rise to a discrete problem of the type

$$\int_{\Omega} \boldsymbol{w}_h \cdot \boldsymbol{y}_h \, d\Omega = \int_{\Omega} \boldsymbol{w}_h \cdot \boldsymbol{y}(\boldsymbol{x}) \, d\Omega \tag{15}$$

we recognize on the left side a mass-like operator $\check{\boldsymbol{M}}$, so that such operation can be understood as

$$\check{\boldsymbol{M}} \boldsymbol{y}_h = \int_{\Omega} \boldsymbol{w}_h \cdot \boldsymbol{y}(\boldsymbol{x}) \, d\Omega \tag{16}$$

If mass lumping techniques are applied to $\check{\boldsymbol{M}}$ a diagonal matrix is defined with each diagonal term representing the nodal area of the corresponding node of the FE mesh. Under such assumption, the projection operator can be approximated as an *area-weighted smoothing* of the original variable. By definition, the orthogonal projection of the variable is the part of the variable that is orthogonal to the FE space, that is, the part that can not be represented onto this space. We can define constructively the orthogonal projector as the operator that takes away from the projected variable everything that can be represented in the FE space. Since the projection operator is linear, this is done as

$$\mathcal{P}^{\perp}(\boldsymbol{y}) := \boldsymbol{y} - \mathcal{P}(\boldsymbol{y}) = \boldsymbol{y} - \boldsymbol{y}_h \tag{17}$$

with this definition is immediately verified that

$$\mathcal{P}^{\perp}\mathcal{P}(\boldsymbol{y}_h) = \mathcal{P}(\boldsymbol{y}_h) - \mathcal{P}(\mathcal{P}(\boldsymbol{y}_h)) = \boldsymbol{y}_h - \boldsymbol{y}_h = \boldsymbol{0} \tag{18}$$

thus proving the orthogonality.

3 Large deformation case

To handle large deformations, the strain $\boldsymbol{\varepsilon}(\mathbf{u})$ needs to be defined as a large strain measure. A natural possibility is to define it as the Almansi strain as $\boldsymbol{\varepsilon}(\mathbf{u}) := \frac{1}{2}(\nabla\mathbf{u} + \nabla^t\mathbf{u} + \nabla\mathbf{u}\nabla^t\mathbf{u})$ where the the gradients are computed with respect to the deformed configuration. The discrete system can then be obtained by integrating Eq. (9) onto the current (deformed) configuration Ω_t, as normally done in Updated Lagrangian approaches.

An equivalent formulation can be obtained by integrating on the reference (undeformed) domain Ω_0, provided that appropriate conjugate strain measures are employed. The equivalent Total Lagrangian formulation can be obtained following the traditional procedure described e.g. in [16]. We followed here this approach in writing our system.

Introducing the Cauchy-Green strain (CG) measure

$$\boldsymbol{E} = \frac{1}{2}(\boldsymbol{F}^T\boldsymbol{F} - \boldsymbol{I}) \tag{19}$$

and a properly defined elasticity tensor $\boldsymbol{C}$ we can compute the second Piola-Kirchhoff (PK2) stress $\boldsymbol{S} = \boldsymbol{C}(\boldsymbol{E}, \boldsymbol{S}) : \boldsymbol{E}$ which completes the informations needed for the evaluation of all terms of interest. The vector of internal forces $\boldsymbol{f}_{int}^0$ can be obtained as

$$\boldsymbol{f}_{int}^0 = \int_{\Omega_0} \boldsymbol{B}_0^T \boldsymbol{S} \, d\Omega_0 \tag{20}$$

where, $\boldsymbol{F} := \dfrac{\partial \boldsymbol{x}}{\partial \boldsymbol{X}}$ is the deformation gradient. Strain variations can be computed on the basis of the operators $\boldsymbol{B}_0$, in the undeformed configuration, and $\boldsymbol{B}$, in the deformed domain.

Matrix $\boldsymbol{B}_0$ (used in the Total Lagrangian approach) is composed of submatrices, each associated with a node I. For a particular node I, the sub-matrix $\boldsymbol{B}_0^I$ is written in Voigt form as:

$$\boldsymbol{B}_0^I = \begin{pmatrix} \dfrac{\partial N_I}{\partial X}\dfrac{\partial x}{\partial X} & \dfrac{\partial N_I}{\partial X}\dfrac{\partial y}{\partial X} \\ \dfrac{\partial N_I}{\partial y}\dfrac{\partial x}{\partial Y} & \dfrac{\partial N_I}{\partial Y}\dfrac{\partial y}{\partial Y} \\ \dfrac{\partial N_I}{\partial X}\dfrac{\partial x}{\partial Y} + \dfrac{\partial N_I}{\partial Y}\dfrac{\partial x}{\partial X} & \dfrac{\partial N_I}{\partial X}\dfrac{\partial y}{\partial Y} + \dfrac{\partial N_I}{\partial Y}\dfrac{\partial y}{\partial X} \end{pmatrix} \tag{21}$$

For the Updated Lagrangian case, the corresponding matrix is $\boldsymbol{B}_t$:

$$\boldsymbol{B}_t^I = \begin{pmatrix} \dfrac{\partial N_I}{\partial x} & 0 \\ 0 & \dfrac{\partial N_I}{\partial y} \\ \dfrac{\partial N_I}{\partial y} & \dfrac{\partial \acute{N}_I}{\partial x} \end{pmatrix} \tag{22}$$

Table 1 summarizes the values of the corresponding terms in Total Lagrangian and Updated Lagrangian approaches.

Table 1 Entities measures in both reference Ω_0 and deformed Ω_t configuration for irreducible and mixed formulation

Entity	Integration domain Ω	
	Total lagrangian Ω_0	Updated lagrangian Ω_t
Strain	(CG) $\boldsymbol{E}(\mathbf{u}_h) := \frac{1}{2}\boldsymbol{F}^T\boldsymbol{F} - \boldsymbol{I}$	(AL) $\boldsymbol{e}(\mathbf{u}_h) := \frac{1}{2}\left(\boldsymbol{I} - \boldsymbol{F}^{-T}\boldsymbol{F}^{-1}\right)$
Projection	$\int_{\Omega_0} \boldsymbol{\gamma}_h \cdot (\boldsymbol{E}_h - \boldsymbol{E}(\boldsymbol{u}_h))\, d\Omega_0 = \boldsymbol{0}$	$\int_{\Omega} \boldsymbol{\gamma}_h \cdot (\boldsymbol{e}_h - \boldsymbol{e}(\boldsymbol{u}_h))\, d\Omega = \boldsymbol{0}$
Stabilized strain	$\boldsymbol{E}^{stab} = (1 - \tau_\epsilon)\boldsymbol{E}_h + \boldsymbol{E}(\boldsymbol{u}_h)$	$\boldsymbol{e}^{stab} = (1 - \tau_\epsilon)\boldsymbol{e}_h + \boldsymbol{e}(\boldsymbol{u}_h)$
Stress (irreducible)	(PK2) $\boldsymbol{S} = \boldsymbol{C}_0 : \boldsymbol{E}$	Cauchy $\boldsymbol{\sigma} = \boldsymbol{C} : \boldsymbol{e}$
Stress (mixed)	(PK2) $\boldsymbol{S}^{stab} = \boldsymbol{C}_0 : \boldsymbol{E}^{stab}$	Cauchy $\boldsymbol{\sigma}^{stab} = \boldsymbol{C} : \boldsymbol{e}^{stab}$
External forces	$\boldsymbol{f}_0^{ext} = \int_{\partial\Omega_0} \boldsymbol{W}_h \cdot \boldsymbol{T}\, d\Gamma_0$	$\boldsymbol{f}^{ext} = \int_{\partial\Omega} \boldsymbol{w}_h \cdot \boldsymbol{t}\, d\Gamma$
Internal forces (irreducible)	$\boldsymbol{f}_0^{int} = \int_{\Omega_0} \boldsymbol{B}_0^T \boldsymbol{S}\, d\Omega_0$ (Voigt Notation)	$\boldsymbol{f}^{int} = \int_{\Omega} \boldsymbol{B}_t^T \boldsymbol{\sigma}\, d\Omega$ (Voigt Notation)
Internal forces (mixed)	$\boldsymbol{f}_0^{int} = \int_{\Omega_0} \boldsymbol{B}_0^T \boldsymbol{S}^{stab}\, d\Omega_0$ (Voigt Notation)	$\boldsymbol{f}^{int} = \int_{\Omega} \boldsymbol{B}_t^T \boldsymbol{\sigma}^{stab}\, d\Omega$ (Voigt Notation)

Fig. 1 Central differences scheme
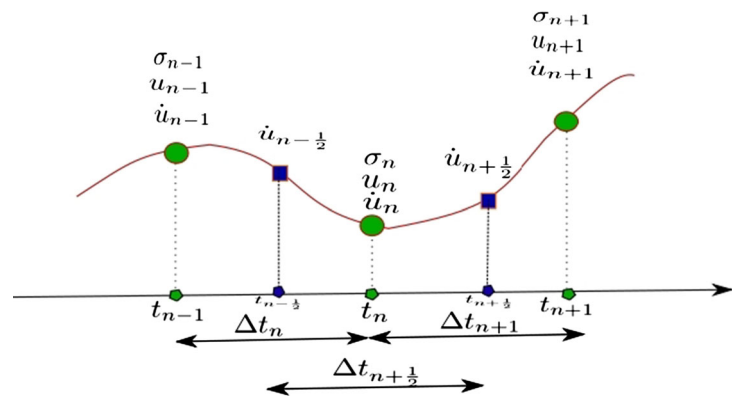
As a final remark, we would like to observe how, in the Total Lagrangian case, it is natural to express the projection operator in terms of $\boldsymbol{E}$ as

$$\int_{\Omega_0} \boldsymbol{\gamma}_h \cdot (\boldsymbol{E}_h - \boldsymbol{E}(\boldsymbol{u}_h))\, d\Omega_0 = \boldsymbol{0} \tag{23}$$

This choice is *not* exactly equivalent to projecting the Almansi strain (AL) $\boldsymbol{e}$ in the deformed domain, but rather corresponds to a slightly different definition of the projection operator. In other words, the corresponding projection operation in the deformed configuration is written as

$$\int_{\Omega} \boldsymbol{\gamma}_h \cdot (\boldsymbol{e}_h - \boldsymbol{e}(\boldsymbol{u}_h))\, d\Omega = \boldsymbol{0} \tag{24}$$

4 Explicit transient integration

To integrate the dynamic balance equation, a time-marching algorithm is needed. Implicit strategies with unconditional stability balance the cost of solving large sparse linear systems with the possibility of using large time steps. Explicit solvers are usually considered advantageous in addressing very short transient phenomena or very high non-linearities.

For the case of the mixed displacement-strain formulation no time derivative is present for the strains, making less straightforward the definition of an explicit technique. The

aim of the next section is to propose a feasible, completely explicit, algorithm for the time integration. Within the same section we also prove that the stability limit for the proposed explicit algorithm is not worse (and generally better) than for the corresponding irreducible formulation. To do this we first recall the standard time integration procedure, and then we develop the integration procedure applied to the mixed formulation described herein.

4.1 Standard formulation in explicit dynamics (irreducible problem)

A commonly used algorithm in the time integration of problems in structural dynamics is the *Central Differences* (CD) time marching scheme. As shown in Fig. (1), the essential idea of the CD is that the dynamic equilibrium is written at time n so to allow the evaluation of the mid-step velocity and successively of the displacements.

If we consider the discrete dynamic equilibrium problem in the form

$$\boldsymbol{M}\ddot{\boldsymbol{u}}_h(t) + \boldsymbol{D}\dot{\boldsymbol{u}}_h(t) + \boldsymbol{f}^{int}(\boldsymbol{u}_h, t) = \boldsymbol{f}^{ext}(t) \tag{25}$$

where $\boldsymbol{M}$ and $\boldsymbol{D}$ are the mass and damping matrices, assumed diagonal, $\boldsymbol{f}^{int}(\boldsymbol{u})$ and $\boldsymbol{f}^{ext}$ are the nodal vector of internal

and external forces, and $\ddot{\boldsymbol{u}}$, $\dot{\boldsymbol{u}}$ and $\boldsymbol{u}$ are the accelerations, velocities and displacements respectively.

Assuming at time step Δt, the straightforward application of the CD to Eq. (25) leads to the procedure

- Compute the acceleration $\ddot{\boldsymbol{u}}_n = \frac{\dot{u}^{n+\frac{1}{2}} - \dot{u}^{n-\frac{1}{2}}}{\Delta t}$
- Evaluate internal and external forces
- Compute the mid-step velocity by solving

$$\dot{\boldsymbol{u}}_{n+\frac{1}{2}} = [2\boldsymbol{M} + \Delta t \boldsymbol{D}]^{-1} \big[(2\boldsymbol{M} - \Delta t \boldsymbol{D}) \dot{\boldsymbol{u}}_{n-\frac{1}{2}} \\ + 2\Delta t (\boldsymbol{f}_n^{ext} - \boldsymbol{f}_n^{int}(\boldsymbol{u}_n)) \big]$$

- Compute end-of-step displacements as $\boldsymbol{u}_{n+1} = \boldsymbol{u}_n + \Delta t \dot{\boldsymbol{u}}_{n+\frac{1}{2}}$

where subscripts n and $n + 1$ are used to indicate quantities at time $t = t_n$ or $t = t_{n+1}$. Note that the inverse of the sum of damping $\boldsymbol{D}$ and mass matrices $\boldsymbol{M}$ is straightforward since they are both taken as diagonal. The critical time step is given by the Courant limit, which is the time necessary for a sound wave to cross the smallest element in the mesh [17]. For the undamped case this critical time step is given by

$$\Delta t_{cr} \leq \frac{2}{\omega_{max}} \tag{26}$$

where ω_{max} is the maximum eigenvalue associated to the system's stiffness matrix. The frequencies of the discrete system are bounded by the maximum frequency, ω_{max}^e of the individual elements. A useful approximation is given by.

$$\omega_{max}^e \approx \frac{2c^e}{l_{min}^e} \; ; \; l_{min}^e = \min_e \{h^e\} \tag{27}$$

where c^e is the elastic dilational wave speed and l_{min}^e is the smallest characteristic element size in the finite element mesh corresponding to the smallest distance between any two element nodes in the discretized model. Therefore, the critical time is finally expressed as:

$$\Delta t_{cr} \approx \frac{l_{min}^e}{c^e} \tag{28}$$

4.2 Mixed formulation in explicit dynamics

If we now focus on the mixed strain-displacement formulation, the discrete equation of motion (25) is replaced by

$$\boldsymbol{M}\ddot{\boldsymbol{u}}_h(t) + \boldsymbol{D}\dot{\boldsymbol{u}}_h(t) + \boldsymbol{f}^{int}(\boldsymbol{\varepsilon}^{stab}, t) = \boldsymbol{f}^{ext}(t) \tag{29}$$

which differs from Eq. (25) in that the internal forces depend on $\boldsymbol{\varepsilon}^{stab}$, i.e

$$\boldsymbol{f}^{int}(\boldsymbol{\varepsilon}^{stab}) = \int_\Omega \boldsymbol{B}^T \boldsymbol{\sigma} d\Omega = \int_\Omega \boldsymbol{B}^T \boldsymbol{C} : \boldsymbol{\varepsilon}^{stab} d\Omega \tag{30}$$

Taking into account the definition of $\boldsymbol{\varepsilon}^{stab}$ given in Eq. (13b) and replacing it into Eqs. (30), (29) can be rewritten as a set of two equations:

$$\boldsymbol{M}\ddot{\boldsymbol{u}}_h(t) + \boldsymbol{D}\dot{\boldsymbol{u}}_h(t) + \overbrace{\boldsymbol{K}_\tau \boldsymbol{u}_h + \boldsymbol{G}_\tau^T \boldsymbol{\varepsilon}_h}^{\boldsymbol{f}^{int}(t)} = \boldsymbol{f}^{ext}(t) \tag{31a}$$

$$\boldsymbol{\breve{G}}\boldsymbol{u}_h - \boldsymbol{\breve{M}}\boldsymbol{\varepsilon}_h = \boldsymbol{0} \tag{31b}$$

where (31a) represents the modified dynamic equilibrium and (31b) tells that $\boldsymbol{\varepsilon}_h$ shall be the projection of $\boldsymbol{\varepsilon}(u)$. In Eqs. (31b), $\boldsymbol{\breve{M}}$ is a diagonal mass matrix associated to the strain field (needed for the computation of the orthogonal projection of the strain variable); $\boldsymbol{G}_\tau$ and $\boldsymbol{\breve{G}}$ are the discrete symmetric gradient operators and $\boldsymbol{K}_\tau$ is the standard stiffness matrix. For any pair of nodes A and B in one element, these matrices can be written as

$$\boldsymbol{\breve{M}}^{AB} = \delta_{AB} \left(\sum^B \int_{\Omega_e} \boldsymbol{N}_A^T \boldsymbol{N}_B d\Omega \right) \tag{32}$$

$$\boldsymbol{G}_\tau^{AB} = (1 - \tau_\epsilon) \int_{\Omega_e} \boldsymbol{B}_A^T \boldsymbol{C}(\varepsilon_{hB}) \boldsymbol{N}_B d\Omega \tag{33}$$

$$\boldsymbol{\breve{G}}^{AB} = \int_{\Omega_e} \boldsymbol{B}_A^T \boldsymbol{N}_B d\Omega \tag{34}$$

$$K_\tau^{AB} = \tau_\epsilon \int_{\Omega_e} \boldsymbol{B}_A^T \boldsymbol{C}(\boldsymbol{\varepsilon}_h) \boldsymbol{B}_B d\Omega \tag{35}$$

where δ_{AB} is the Kronecker delta ($\delta_{AB} = 1$ for $A = B$, $\delta_{AB} = 0$ if $A \neq B$).

It is convenient to rewrite Eqs. (31a) and (31b) as

$$\begin{pmatrix} \boldsymbol{M} & \boldsymbol{0} \\ \boldsymbol{0} & \boldsymbol{0} \end{pmatrix} \begin{pmatrix} \ddot{\boldsymbol{u}} \\ \boldsymbol{0} \end{pmatrix} + \begin{pmatrix} \boldsymbol{D} & \boldsymbol{0} \\ \boldsymbol{0} & \boldsymbol{0} \end{pmatrix} \begin{pmatrix} \dot{\boldsymbol{u}} \\ \boldsymbol{0} \end{pmatrix} + \begin{pmatrix} \boldsymbol{K}_\tau & \boldsymbol{G}_\tau^T \\ \boldsymbol{\breve{G}} & -\boldsymbol{\breve{M}} \end{pmatrix} \begin{pmatrix} \boldsymbol{u} \\ \boldsymbol{\varepsilon}_h \end{pmatrix} = \begin{pmatrix} \boldsymbol{f}^{ext} \\ \boldsymbol{0} \end{pmatrix} \tag{36}$$

Since this form will make easier eigenvalue computations in the calculation of the critical time step. For this reason we introduce the matrices

$$\boldsymbol{K}_{mixed} := \begin{pmatrix} \boldsymbol{K}_\tau & \boldsymbol{G}_\tau^T \\ \boldsymbol{\breve{G}} & -\boldsymbol{\breve{M}} \end{pmatrix} \tag{37}$$

$$\boldsymbol{M}_{mixed} := \begin{pmatrix} \boldsymbol{M} & \boldsymbol{0} \\ \boldsymbol{0} & \boldsymbol{0} \end{pmatrix} \tag{38}$$

which we will use in the next section. Written in this form, the discrete system is very similar to the one developed for the irreducible case, except that two independent unknowns variables, i.e, the nodal displacement field $\boldsymbol{u_h}$ and the nodal strain field $\boldsymbol{\varepsilon}_h$ are now considered. We can however observe that since $\boldsymbol{\breve{M}}$ is diagonal and Eq. (31b) does not present any time dependence, we can formally express the continuous strain as a function of the displacements field as, $\boldsymbol{\varepsilon_h} = \boldsymbol{\breve{M}}_\tau^{-1} \boldsymbol{\breve{G}} \boldsymbol{u}$ and substitute it into the equilibrium Eq. (31a). By introducing the new symbol

$$\overline{\boldsymbol{K}} := \boldsymbol{K}_\tau + \boldsymbol{G}_\tau^T \boldsymbol{\breve{M}}_\tau^{-1} \boldsymbol{\breve{G}} \tag{39}$$

we can thus rewrite Eq. (31a) in terms of displacements only in the equivalent form

$$M\ddot{u}_h(t) + D\dot{u}_h(t) + \overline{K}u_h = f^{ext}(t) \quad (40)$$

the resulting time integration procedure can be then developed similarly to the irreducible case as

- Compute the acceleration $\ddot{u}_n = \frac{\dot{u}^{n+\frac{1}{2}} - \dot{u}^{n-\frac{1}{2}}}{\Delta t}$.
- Evaluate on every element the discontinuous strain $\varepsilon(u)$.
- Evaluate the strain $\varepsilon_h = \mathcal{P}(\varepsilon(u))$, that is, $\varepsilon_h = \check{M}_\tau^{-1} \check{G}u$.
- Compute internal forces taking into account the stabilized strain.
- Compute the mid-step velocity by solving

$$\dot{u}_{n+\frac{1}{2}} = [2M + \Delta t D]^{-1}[(2M - \Delta t D)\dot{u}_{n-\frac{1}{2}} + 2\Delta t(f_n^{ext} - f_n^{int}(u_n, \varepsilon_n^{stab}))].$$

- Compute end-of-step displacements as $u_{n+1} = u_n + \Delta t \dot{u}_{n+\frac{1}{2}}$.

We remark that, since the computation of the projections is very cheap, the cost per time step of the proposed scheme is very similar to that of the original irreducible algorithm, making it very interesting in view of the accuracy advantage guaranteed by the mixed formulation. In the next subsection we discuss the critical time step for the proposed algorithm, considering first a 1D case, for which an analytical estimate is obtained. We then consider a 2D mesh and provide a numerical verification of the formula.

Before proceeding we would also like to point out that the form used in writing the discrete system obtained is slightly different from the one employed in [7], in that in the current approach the $\check{M}$ is purely diagonal. The approach we follow stems out of using a nodal integration rule in the calculation of the projection and by noticing that the resulting mass term is block diagonal and can thus be solved analytically block by block to make it diagonal. We also observe that this approach is not appealing for the implicit case since it results in a non-symmetric matrix.

4.3 Stability of the explicit mixed formulation

4.3.1 1D mixed bar problem

Let us consider the one-dimensional problem in Fig. (2). This corresponds to a bar with unit cross section, discretized using two elements of length h. Constant material properties Young's modulus E and density ρ are assumed. The degrees of freedom of displacement u_1 and u_3 are fixed for the nodes 1 and 3. For irreducible case, the system's fundamental frequency is given by:
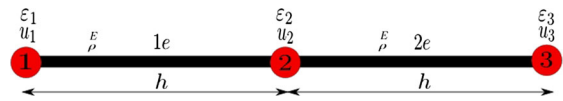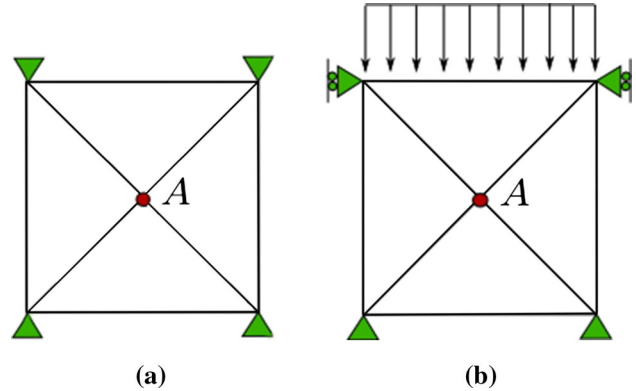

Fig. 2 One-dimensional bar example

Fig. 3 2D case test **a** 2D case test for stability analysis **b** 2D case test for checking second order time accuracy

$$\omega_{irre} = \sqrt{\frac{2E}{\rho h^2}} \quad (41)$$

It is possible to compute analytically the eigenvalues of the mixed problem by evaluating the eigenvalues of the corresponding discrete system. Here A and B represent the local nodes corresponding to the two ends of a 1D bar element. The same linear interpolation function N are used for the strain and displacement fields. Applying the mixed formulation, the local mixed stiffness matrix K_{mixed}^{AB} of a bar mixed element is a 4×4 matrix composed by terms affecting degrees of freedom of displacements and strains. The sub-matrices $\check{M}, \check{G}$, G_τ and K_τ defined in (32–35) for a bar mixed element are

$$\check{M}^{AB} = \frac{h}{2}\begin{pmatrix} 1 & 0 \\ 0 & 1 \end{pmatrix} \quad (42)$$

$$K_\tau^{AB} = \tau_\epsilon \frac{E}{h}\begin{pmatrix} 1 & -1 \\ -1 & 1 \end{pmatrix} \quad (43)$$

$$\check{G}^{AB} = \frac{1}{2}\begin{pmatrix} -1 & -1 \\ 1 & 1 \end{pmatrix} \quad (44)$$

$$G_\tau^{AB} = \frac{E(1-\tau_\epsilon)}{2}\begin{pmatrix} -1 & -1 \\ 1 & 1 \end{pmatrix} \quad (45)$$

The mass matrix for each mixed bar element is trivially computed as

$$M^{AB} = \frac{\rho h}{2}\begin{pmatrix} 1 & 0 \\ 0 & 1 \end{pmatrix} \quad (46)$$

Accordingly, the local mixed stiffness matrix K_{mixed} of a bar element is the assembly of these matrices. Hence, using
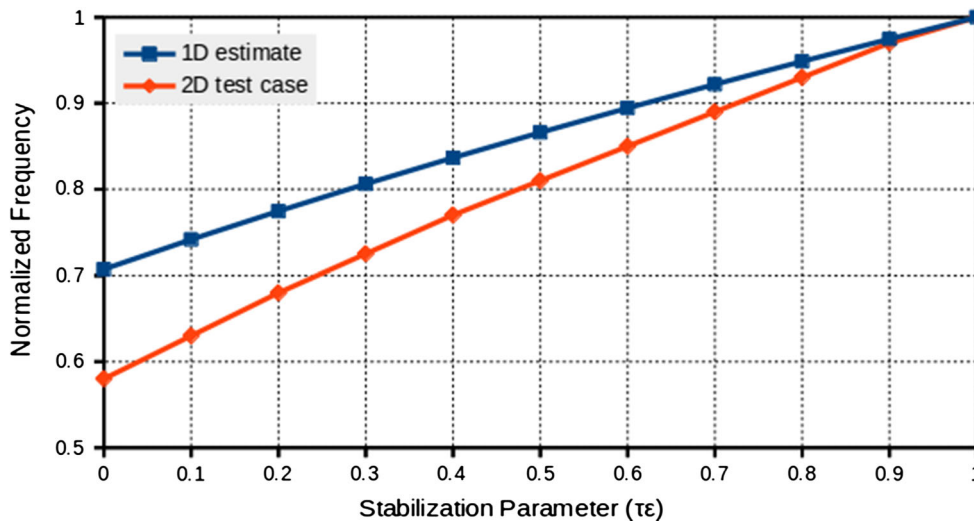
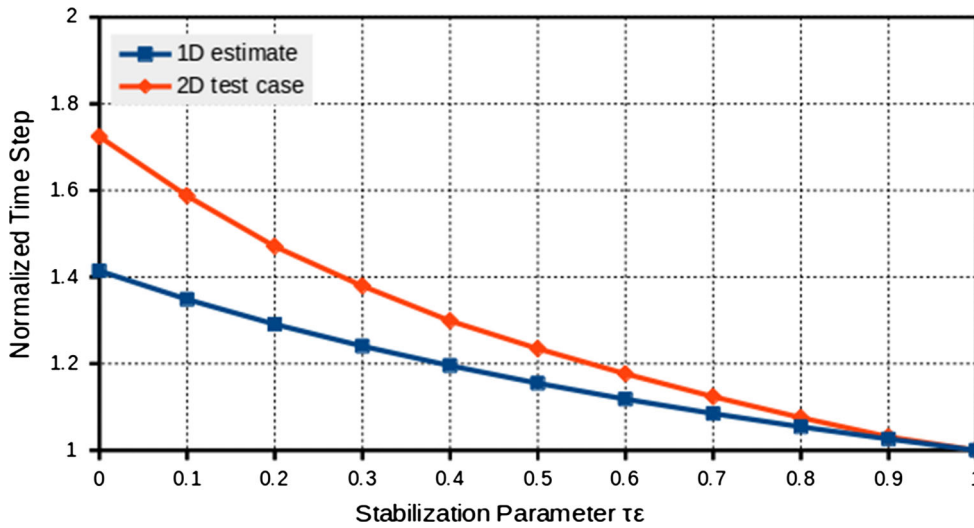**Fig. 4** Variation of normalized frequency with stabilization parameter

Fig. 5 Variation of normalized time step with stabilization parameter

the expression in Eq. (37), it can finally express the mixed local stiffness matrix of a bar element

$$
\boldsymbol{K}_{mixed}^{AB} = \begin{pmatrix} \frac{E\tau_\epsilon}{h} & \frac{-E\tau_\epsilon}{h} & \frac{E(\tau_\epsilon-1)}{2} & -\frac{E\tau_\epsilon}{2} \\ \frac{-E\tau_\epsilon}{h} & \frac{E\tau_\epsilon}{h} & \frac{E(\tau_\epsilon-1)}{2} & -\frac{E(\tau_\epsilon-1)}{2} \\ -\frac{1}{2} & -\frac{1}{2} & -\frac{h}{2} & 0 \\ \frac{1}{2} & \frac{1}{2} & 0 & -\frac{h}{2} \end{pmatrix} \tag{47}
$$

Assembling the elemental contribution of both $\boldsymbol{K}_{mixed}$ and $\boldsymbol{M}_{mixed}$ and fixing the displacements of node 1 and 3, we can obtain the relevant natural frequencies by solving

$$
det(\boldsymbol{K}_{mixed} - \lambda \boldsymbol{M}_{mixed}) = 0
$$
$$
\omega_{mixed}^2 = \lambda \tag{48}
$$

Therefore, after some algebra we obtain the following analytical expression for the first frequency of the mixed system:

$$
\omega_{mixed} = \sqrt{\frac{E(1+\tau_\epsilon)}{\rho h^2}} \tag{49}
$$

As expected the irreducible solution (see Eq. (41)) can be recovered for $\tau_\epsilon = 1$ (which is the limit case at which only the discontinuous strain is taken into account).

4.3.2 2D case

Consider now a $2D$ benchmark example, described in Fig. (3a) to verify numerically that the $1D$ predictions also apply to the $2D$ case. The model is a unit square 1×1 and is discretized in four elements. The corner nodes are fixed. Density
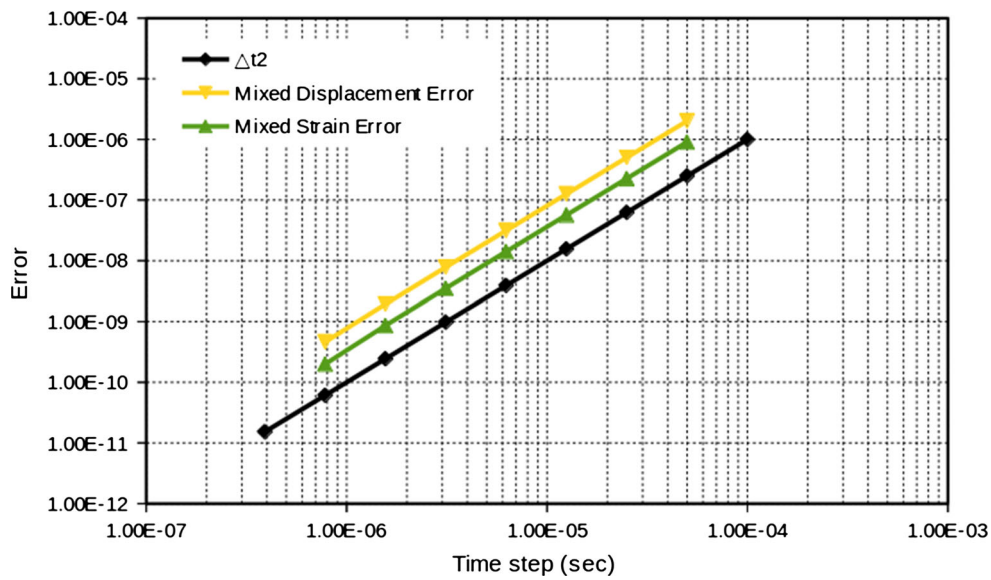
Fig. 6 Time error mixed explicit formulation

Fig. 7 3D dimension view of cantilever beam
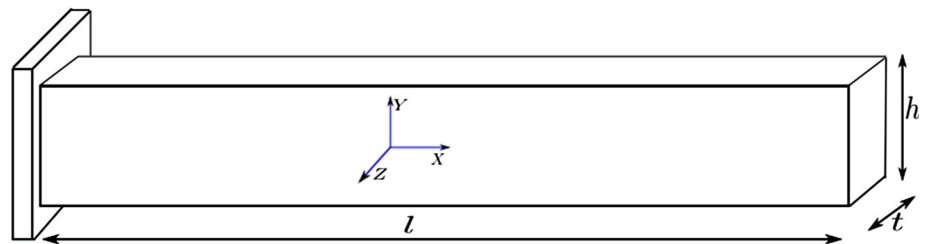
ρ, Young's modulus E, thickness t and Poisson ratio ν are 100 kg, 10^6 N/m^2, 1 m and 0.3 respectively. As the above example, a modal analysis is performed for irreducible and mixed formulation.

The plot of $\omega_{mixed}/\omega_{irre}$, for varying values of the stabilization parameter is given in Fig. (4). Here ω represents here the highest frequency in the system. As predicted by the theoretical analysis, the system becomes more and more flexible as the stabilization parameter decreases, to reach a minimal frequency of about half that of the original irreducible model when the stabilization parameter approaches zero. The immediate implication is that the critical time step for the explicit dynamic analysis is greater for the mixed formulation than for the irreducible one. The numerical experiments shown in Fig. (5) show that, the estimated gain for the two-dimensional case is even more favourable than for the one-dimensional case.

The simple mesh considered here is also suitable to verify that second order time accuracy is retained by the modified algorithm. To verify this fact, we slightly modify the boundary conditions and consider the settings shown in Fig. (3b). A dynamic analysis is performed, comparing the mixed and the irreducible formulation. Since a Lagrangian approach is followed, the spatial error and the time integration error

Table 2 Material and Geometric data for the dynamic analysis of the cantilever beam

Material and geometric data	Value ($N - m$)
Young's modulus E	2.0 GPa
Poisson's ratio υ	0.2
Density ρ	1,000.00 Kg/m^3
Length l	5.00 m
Cross section A	0.25 m^2
Inertia I	2.604167×10^{-3} m^4
Thickness t	0.25 m
Gravity g	9.80665 m/s^2

are decoupled. We can hence compute a reference solution employing an extremely small time step. We then compute the solution using different time steps and sample the values of displacement and strain at the point A of Fig. (3b) at the time instant t=0.4 s. By comparing the results to the reference we can then plot (in logarithmic scale) the error as a function of the employed time step size. Since the curve Δt^2 shown in Fig. (6) is parallel to the error plot, the graph proves the expected convergence rates.

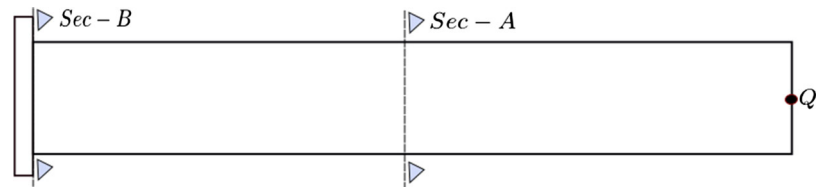**Fig. 8** Boundary conditions for small deformations in cantilever beam and section cuts

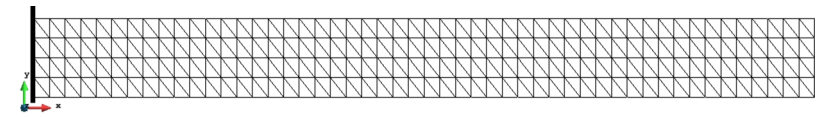**Fig. 9** Finite element mesh of cantilever beam model. Mesh *A*

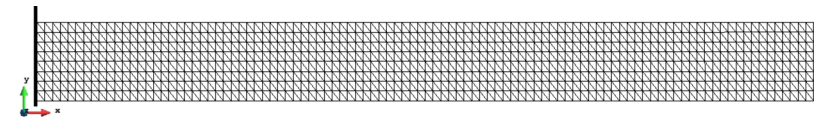**Fig. 10** Finite element mesh of cantilever beam model. Mesh *B*

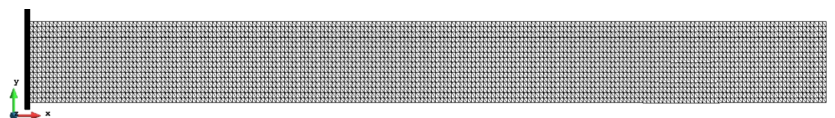**Fig. 11** Finite element mesh of cantilever beam model. Mesh *C*

Table 3 Discretization data for Mesh *A*, *B* and *C*

Discretization data		
Mesh type	Number of nodes	Number of elements
Mesh A	255	400
Mesh B	909	1, 600
Mesh C	3,417	6,400

4.4 Numerical accuracy of the mixed formulation

In this section the accuracy of the proposed mixed explicit formulation is assessed in the application to a real transient dynamic problem, in both small and large deformations. The test case consists of a cantilever beam with the geometrical dimensions described in the Fig. 7 and Table 2. The displacements are completely constrained at the left side. Material parameters are given in Table 2. In order to obtain comparable results, the same time step was employed for the mixed and irreducible approaches. A reference solution was computed employing a very dense finite element mesh (and consequently a very small time step). Calculations are performed with the Multi-physics finite element program KRATOS [18,19], developed at the International Center for Numerical Methods in Engineering (CIMNE). Pre and post-processing is done with GiD, also developed at CIMNE [20].

4.4.1 Dynamic cantilever beam. Small deformations case.

We begin by considering a small deformation case. According to Bernoulli's beam theory, the maximum static deflection δ_{max}^{st} of a cantilever beam under its own weight occurs at

its free end (Eq. 50a). Under the same assumptions, the first natural frequency ω_1 of the same beam is given in Eq. 50b.

$$\delta_{max}^{st} = u_{max} = \frac{\rho g A l^4}{8EI} \tag{50a}$$

$$\omega_1 = 1.875^2 \sqrt{\frac{EI}{\rho A l^4}} \tag{50b}$$

For the dynamic case, the maximum dynamic deflection δ_{max}^{din} is expected to be exactly twice the value of the maximum static deflection. For the test we consider three different structured triangle meshes *A*, *B* and *C* depicted in the Figs. 9, 10 and 11 respectively. Details of discretization are shown in the Table 3.

The analytical maximum static deflection δ_{max}^{st} and the first natural frequency ω_1 is 18.3875 mm and 28.705 rad/s respectively. The corresponding period *T* of this frequency is 0.219 s. A linear step-by-step dynamic analysis is done using *CD* for both irreducible and mixed formulation. The results of the analysis are depicted in Figs. 12, 13 and 14. They correspond to absolute values of vertical displacement (displacement Y direction) evolution at free end (point Q in Fig. 8). As expected, for values of τ_ε in the typical range 0.1-0.5, at any given mesh resolution, the mixed formulation is slightly more accurate than the irreducible one. This is true both in terms of phase accuracy and in terms of stiffness. Interestingly, depending on the value of the stabilization parameter the structure can be either too flexible or too stiff compared to the analytical solution, which is not unexpected since a mixed-formulation may converge from either side. As expected, as the mesh is refined, all formulations converge to the reference solution.
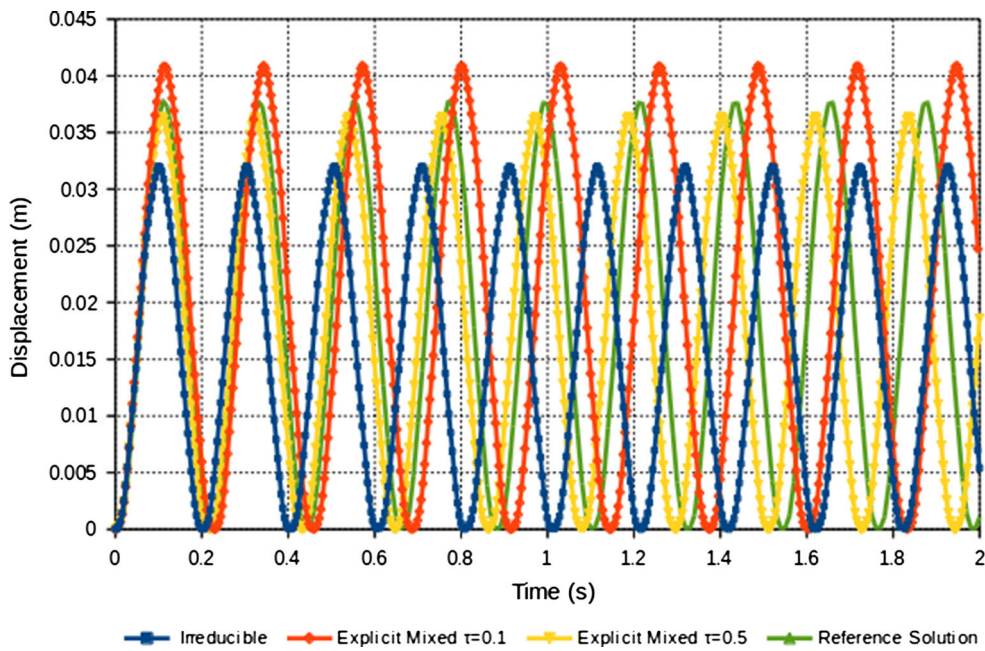
Fig. 12 Step-by-step dynamic analysis using both irreducible and mixed explicit formulation for mesh A
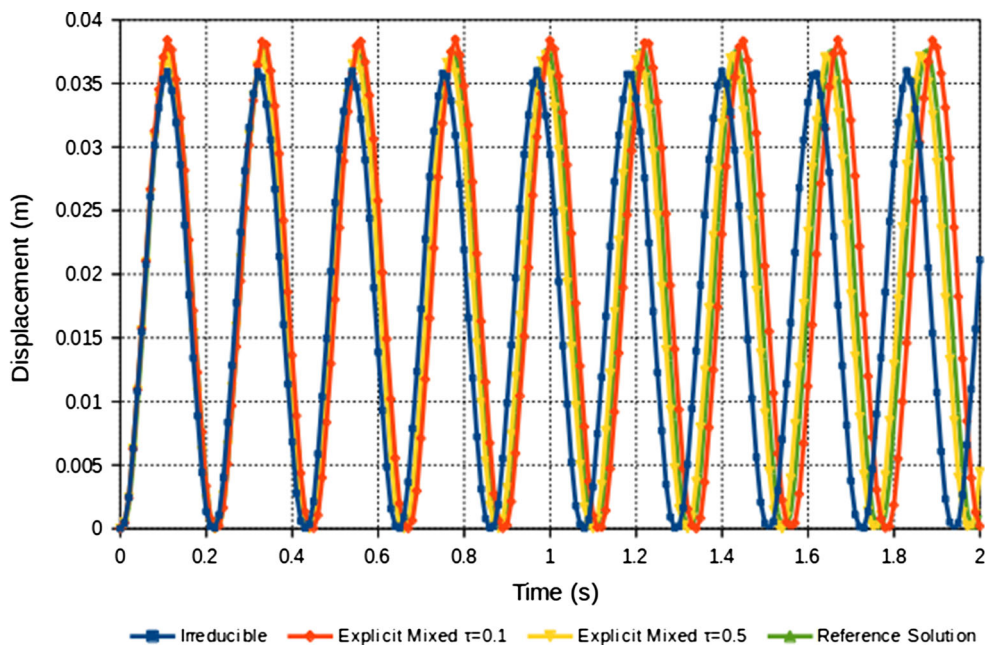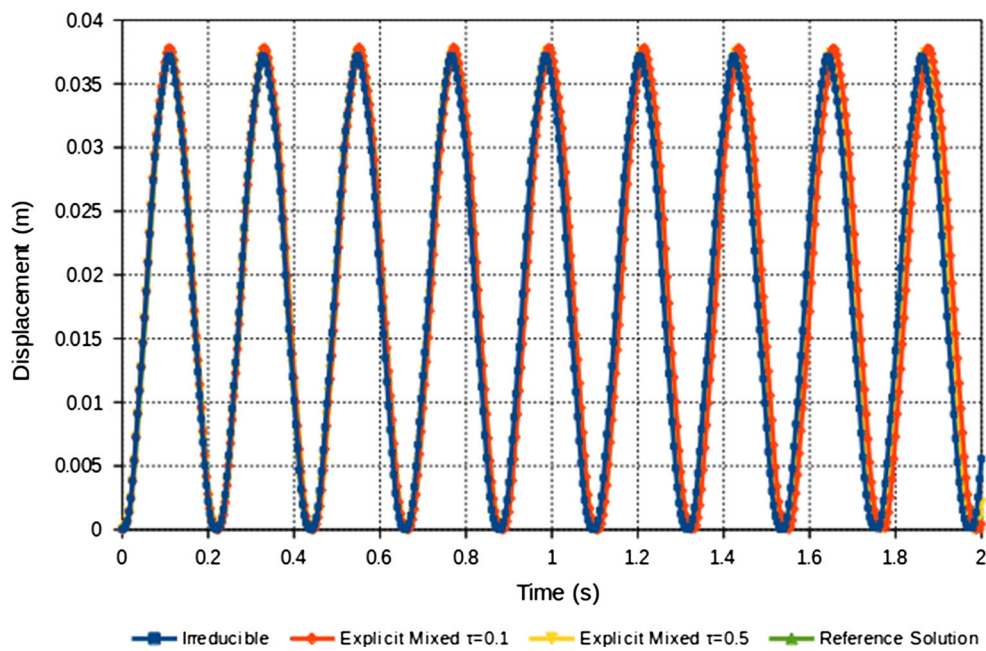

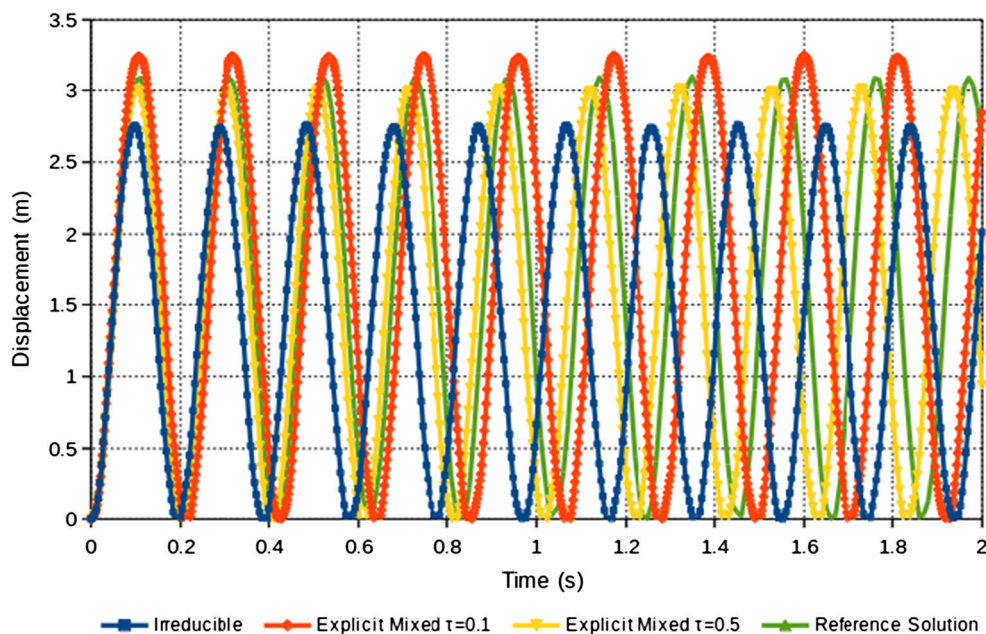**Fig. 13** Step-by-step dynamic analysis using both irreducible and mixed explicit formulation for mesh B

As a remark we observe that as shown in previous works[7, 8, 15], where the static case was explored, the explicit mixed formulation is always (independently on the τ_ε) more accurate than the irreducible formulation on a given mesh.

4.4.2 Dynamic cantilever beam. Large deformations case

As a second example, we consider the same settings and increase by a factor 100 the applied load (100 times higher

gravity load), thus triggering a large deformation response. The results shown in Figs. 15, 16 and 17 depicts the displacement of the tip (intended as the center point of the rightmost face) for the three meshes identified as *A*, *B* and *C*.

As it can be expected convergence is guaranteed, even for large deformations cases using a mixed-explicit Total Lagrangian approach. It is also interesting to compare the irreducible and mixed formulations Green-Lagrange strain

Fig. 14 Step-by-step dynamic analysis using both irreducible and mixed explicit formulation for mesh C

Fig. 15 Step-by-step dynamic analysis using both irreducible and mixed CD scheme for mesh A

distributions over two different cross sections as shown in Fig. 8.

The strain distribution in the middle-right section and at the constraint is shown in Figs. 18 and 19 for mesh A, 20 and 21 for mesh B and 22 and 23 for mesh C.

As the images suggest, and in accordance to the theory, the strain spatial convergence is faster for the mixed formulation than for the irreducible one. Note that already for the structured non-symmetric coarse mesh (mesh A), the distri-

bution of strains in the section gives sensibly better results with respect to the irreducible one. The strain distribution also appears to converge faster to the reference result as the mesh is refined.

Applying the mixed formulation, in Figs. 24, 25 and 26 we observe how the imposed load excites the first, second and third modes of the beam. As expected, if a finer discretization is used more vibration modes appear in the analysis.
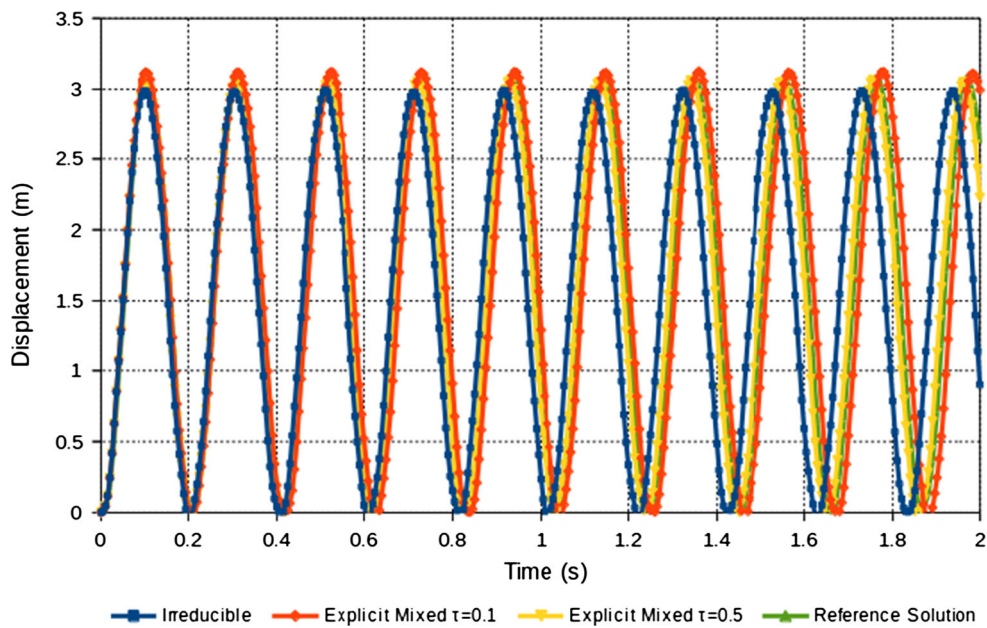
Fig. 16 Step-by-step dynamic analysis using both irreducible and mixed CD scheme for mesh B
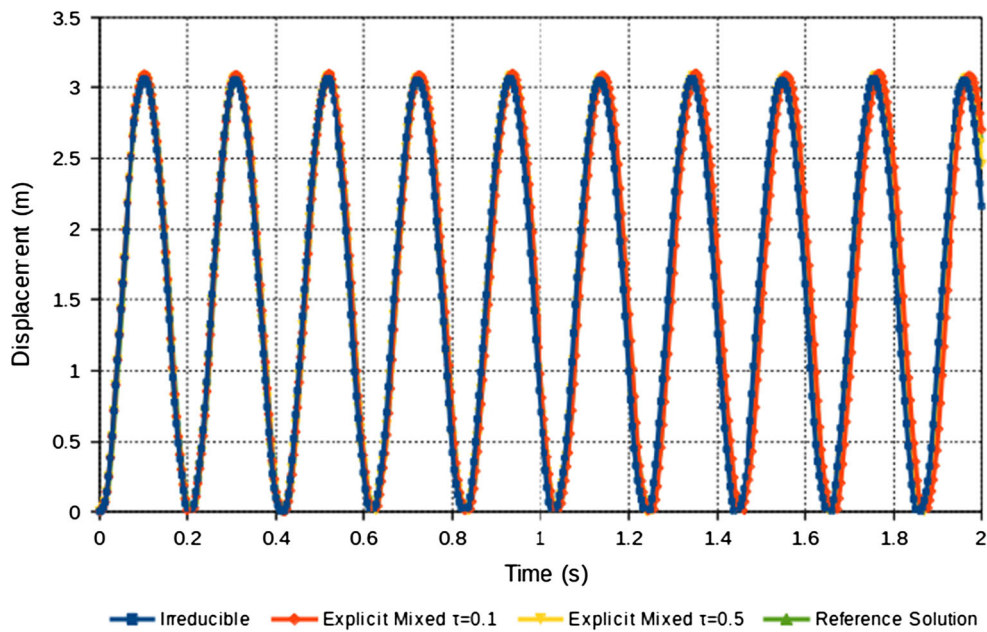

Fig. 17 Step-by-step dynamic analysis using both irreducible and mixed CD scheme for mesh C

Since the stability analysis developed is only valid for the linear case, we experimentally increased the time step used in the analysis until the method failed, so to approximate the largest possible time step. The results are shown in Table 4 together with the time step for one-dimensional mixed and irreducible case. We approximate the length of the triangular element l_e as the half-root square of the quadrilateral area closed by the triangle, i.e; $l_e = \frac{1}{2}\sqrt{bh}$. As we can

note, even for large deformation case the time step used in the mixed-explicit formulation is larger than irreducible one, closely following the predictions in Fig. 5. Specifically we numerically verify that the stable time step for this example is at least a factor of 1.43 larger for the mixed formulation than for the original irreducible one, which represents a very important performance gain for the proposed formulation.
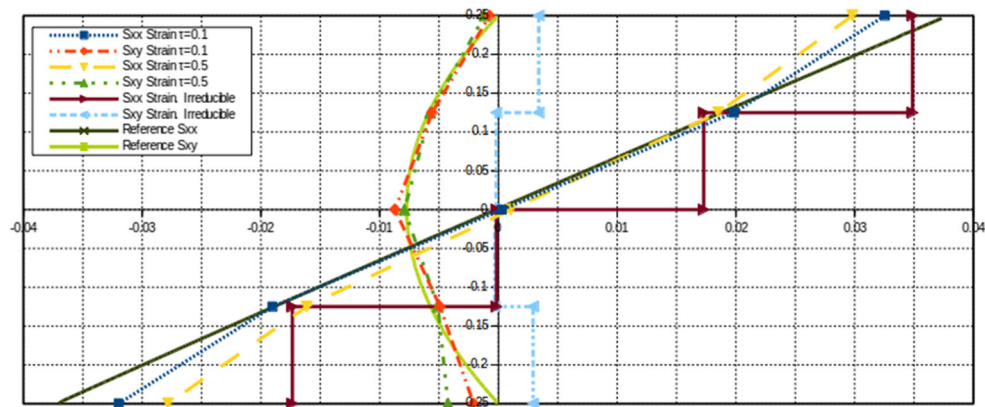
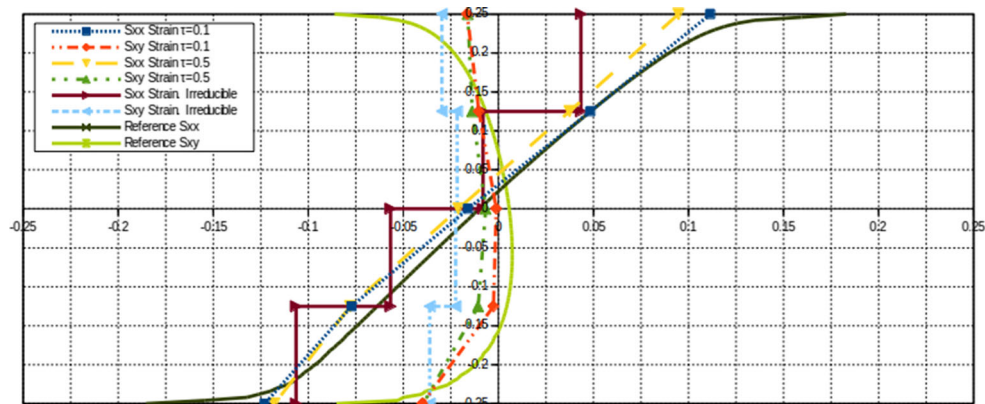**Fig. 18** Section A normal and shear strain distribution at maximum displacement for mesh *A*

Fig. 19 Section B normal and shear strain distribution at maximum displacement for mesh *A*
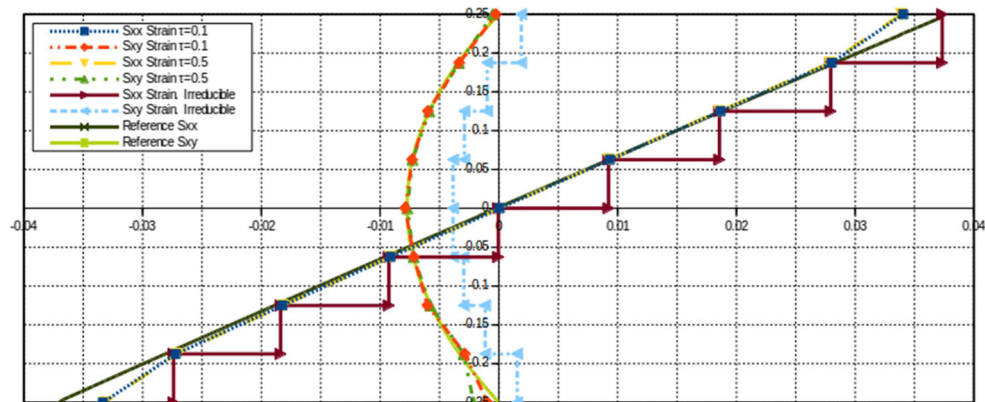

Fig. 20 Section A normal and shear strain distribution at maximum displacement for mesh *B*

5 Conclusion

This paper presents the formulation of a stable, OSS based, mixed explicit strain/displacement formulation for the solution of linear and non-linear problems is solid mechanics. In the work we describe a simple algorithm allowing the explicit time integration of such mixed formulation. The resulting explicit scheme retains second order accuracy in time and has a favourable stability estimate when compared to the irreducible formulation. The numerical results also show how the results obtained compare favourably in terms of accuracy with the corresponding irreducible formulations at any mesh resolution. The advantage is particularly evident in the strain predictions.
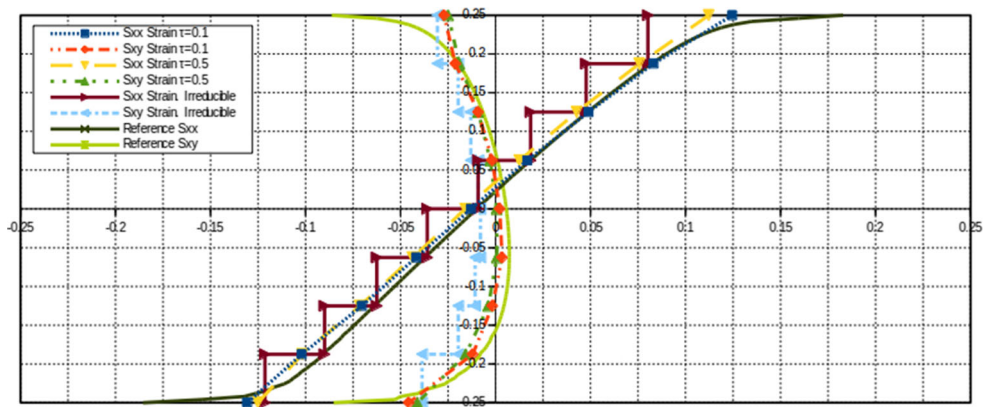
Fig. 21 Section B normal and shear strain distribution at maximum displacement for mesh *B*
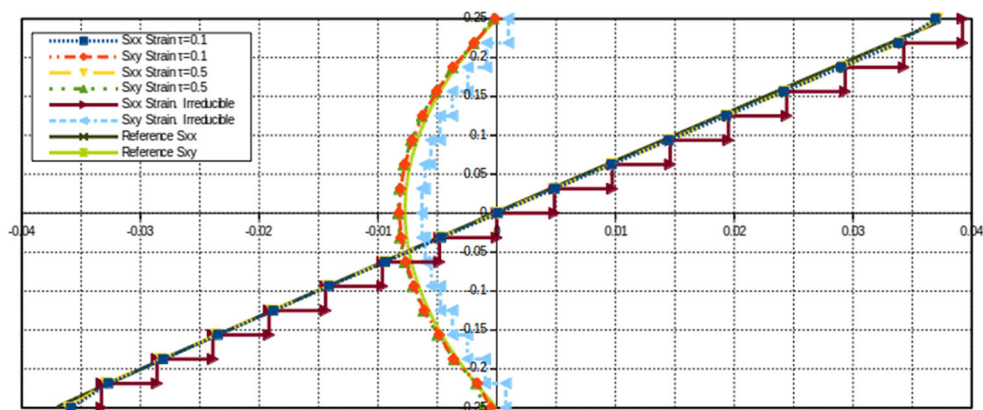

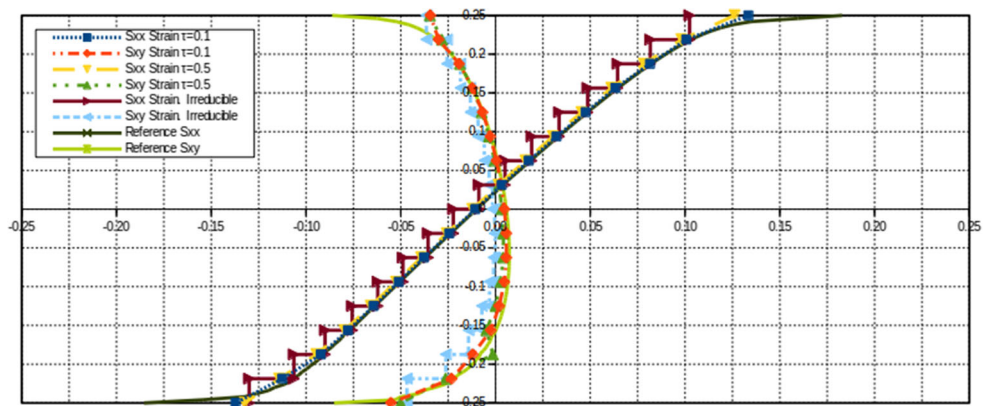**Fig. 22** Section A normal and shear strain distribution at maximum displacement for mesh *C*

Fig. 23 Section B normal and shear strain distribution at maximum displacement for mesh *C*

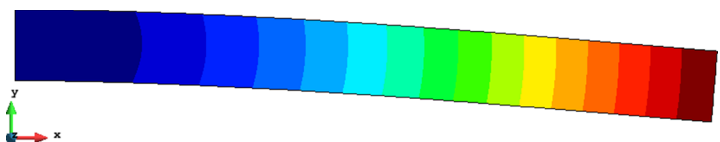**Fig. 24** First vibration mode of the cantilever beam in mesh *C*

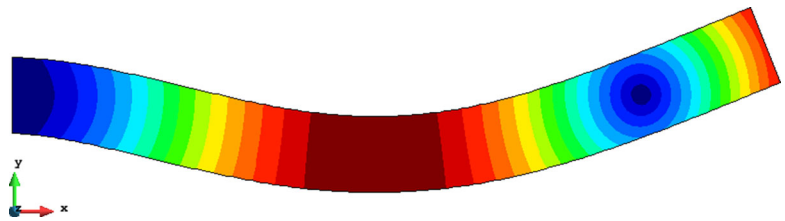**Fig. 25** Second vibration mode of the cantilever beam in mesh *C*

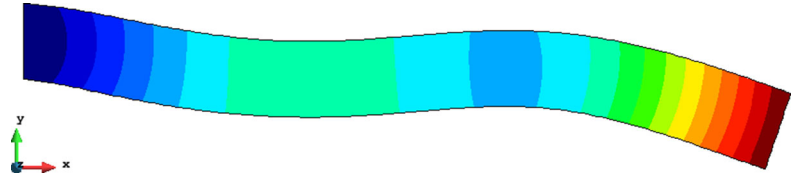**Fig. 26** Third vibration mode of the cantilever beam in mesh *C*

Table 4 Maximum Δt^{max} for analysis in irreducible and mixed formulation

Critical Δt^{max} computed

Mesh type	Δt^{max} irreducible 1D (s)	Δt^{max} irreducible (s)	Δt^{max} mixed 1D (s)	Δt^{max} mixed (s)	Factor
Mesh A	1.76e−04	5.30e−05	2.38e−04	7.585e−05	1.43
Mesh B	8.83e−05	2.55e−05	1.19e−04	3.795e−05	1.49
Mesh C	4.41e−05	1.07e−05	5.95e−05	1.80e−05	1.68

References

1. de Souza NetoEA, Andrade PiresFM, Owen DRJ (2005) F-bar-based linear triangles and tetrahedra for finite strain analysis of nearly incompressible solids. Part I: formulation and benchmarking. Int J Numer Methods Eng 62(3):353–383
2. Gil Antonio J, Hean Lee Chun, Bonet Javier, Aguirre Miquel (2014) Stabilised petrov-galerkin formulation for linear tetrahedral elements in compressible, nearly incompressible and truly incompressible fast dynamics. Comput Methods Appl Mech Eng 276:659–690
3. David S Malkus, Hughes Thomas JR (1978) Mixed finite element methods—reduced and selective integration techniques: a unification of concepts. Comput Methods Appl Mech Eng 15(1):63–81
4. Simo JC, Taylor RL, Pister KS (1985) Variational and projection methods for the volume constraint in finite deformation elasto-plasticity. Comput Methods Appl Mech Eng 51(1–3):177–208
5. Taylor Robert L (2000) A mixed-enhanced formulation tetrahedral finite elements. Int J Numer Methods Eng 47(1–3):205–227
6. Scovazzi G (2012) Lagrangian shock hydrodynamics on tetrahedral meshes: a stable and accurate variational multiscale approach. J Comput Phys 231(24):8029–8069
7. Cervera M, Chiumenti M, Codina R (2010) Mixed stabilized finite element methods in nonlinear solid mechanics: part I: formulation. Comput Methods Appl Mech Eng 199(37–40):2559–2570
8. Cervera M, Chiumenti M, Codina R (2010) Mixed stabilized finite element methods in nonlinear solid mechanics: part II: Strain localization. Comput Methods Appl Mech Eng 199(37–40):2571–2589
9. Codina R (2002) Stabilized finite element approximation of transient incompressible flows using orthogonal subscales. Comput Methods Appl Mech Eng 191(39–40):4295–4321
10. Donea Jean, Huerta Antonio (2003) Finite element methods for flow problems, 1st edn. Wiley, Chichester
11. Hughes Thomas JR (1995) Multiscale phenomena: Green's functions, the dirichlet-to-neumann formulation, subgrid scale models, bubbles and the origins of stabilized methods. Comput Methods Appl Mech Eng 127(1–4):387–401
12. Oñate E, Valls A, García J (2006) FIC/FEM formulation with matrix stabilizing terms for incompressible flows at low and high reynolds numbers. Comput Mech 38(4–5):440–455
13. Hughes Thomas J R, Scovazzi Guglielmo, Franca Leopoldo P (2004) Multiscale and stabilized methods. Wiley, New York
14. Hughes Thomas JR, Feijóo Gonzalo R, Mazzei Luca, Quincy Jean-Baptiste (1998) The variational multiscale method-a paradigm for computational mechanics. Comput Methods Appl Mech Eng 166(1—-2):3–24 Advances in Stabilized Methods in Computational Mechanics
15. Cervera M, Chiumenti M, Codina R (2011) Mesh objective modeling of cracks using continuous linear strain and displacement interpolations. Int J Numer Methods Eng 87(10):962–987
16. Belytschko T, Liu WK, Moran B (2000) Nonlinear finite elements for continua and structures. Wiley, New York
17. Har Jason, Fulton Robert E (2003) A parallel finite element procedure for contact-impact problems. Eng Comput 19:67–84. doi:10.1007/s00366-003-0252-4
18. Dadvand P, Rossi R, Gil M, Martorell X, Cotela J, Juanpere E, Idelsohn SR, Oñate E (2013) Migration of a generic multi-physics framework to HPC environments. Comput Fluids 80(0):301–309
19. Dadvand P, Rossi R, Oñate E (2010) An object-oriented environment for developing finite element codes for multi-disciplinary applications. Arch Comput Methods Eng 17(3):253–297
20. GiD (2009) The personal pre and post processor
21. Brezzi F, Fortin M, Marini D (1991) Mixed finite element methods. Springer, New York

22. Codina R (2000) Stabilization of incompresssibility and convection through orthogonal sub-scales in finite elements methods. Comput Meth Appl Mech Eng 190:1579–1599

23. Codina R (2008) Analysis of a stabilized finite element approximation of the oseen equations using orthogonal subscales. Appl Numer Math 58(3):264–283

24. Larese A, Rossi R, Oñate E, Idelsohn SR (2012) A coupled pfem-eulerian approach for the solution of porous FSI problems. Comput Mech 50(6):805–819

25. Larese A, Rossi R, Oñate E, Toledo M, Morán R, Campos H. Numerical and experimental study of overtopping and failure of rockfill dams. International Journal of Geomechanics, 0(0):04014060, 0

26. Zienkiewicz OC, Taylor RL, Zhu JZ (2005) The finite element method: its basis and fundamentals, 6th edn. Butterworth-Heinemann, Oxford

27. Zienkiewicz, OC, Taylor, RL, Baynham, JAW (1983) Mixed and irreducible formulations in finite element analysis, in hybrid and mixed finite element methods. In: Atlury SN, Gallagher RH, Zienkiewicz OC (eds.). Wiley, New York

28. Arnold Douglas N (1990) Mixed finite element methods for elliptic problems. Comput Methods Appl Mech Eng 82(1—-3):281–300 Proceedings of the Workshop on Reliability in Computational Mechanics

29. Arnold Douglas N, Winther Ragnar (2003) Mixed finite elements for elasticity in the stress-displacement formulation. Contemp Math 239:33–42 n Z. Chen, R. Glowinski, and K. Li, editors, Current trends in scientific computing (Xi'an, 2002)

30. Arnold Douglas N, Winther Ragnar (2002) Mixed finite elements for elasticity. Numerische Mathematik 92(3):401–419

31. Oñate E, Rojek J, Taylor RL, Zienkiewicz OC (2004) Finite calculus formulation for incompressible solids using linear triangles and tetrahedra. Int J Numer Methods Eng 59(11):1473–1500